Journal of Biomolecular NMR **27:** 351–364, 2003.
KLUWER/ESCOM

Measurement of methyl ^{13}C-^{1}H cross-correlation in uniformly ^{13}C-, ^{15}N-, labeled proteins

Weidong Liu[a], Yu Zheng[a], David P. Cistola[b] & Daiwen Yang[a,*]
[a]*Department of Biological Sciences and Department of Chemistry, National University of Singapore, 4 Science Drive, 117543, Singapore;* [b]*Department of Biochemistry and Molecular Biophysics, Washington University School of Medicine, 660 South Euclid Avenue, Campus Box 8231, St. Louis, MO 63110, U.S.A.*

Received 14 April 2003; Accepted 24 June 2003

Key words: cross-correlated relaxation, fatty acid binding protein, methyl dynamics, order parameter

Abstract

An understanding of side chain motions in protein is of great interest since side chains often play an important role in protein folding and intermolecular interactions. A novel method for measuring the dynamics of methyl groups in uniformly ^{13}C-, ^{15}N-labeled proteins has been developed by our group. The method relies on the difference in peak intensities of ^{13}C quartet components of methyl groups, in a spectrum recording the free evolution of ^{13}C under proton coupling in a constant-time period. Cross-correlated relaxation rates between ^{13}C-^{1}H dipoles can be easily measured from the intensities of the multiplet components. The degree of the methyl restrictions (S'^2) can be estimated from the cross-correlated relaxation rate. The method is demonstrated on a sample of human fatty acid binding protein in the absence of fatty acid. We obtained relaxation data for 33 out of 46 residues having methyl groups in apo-IFABP. It has been found that the magnitude of the CSA tensor of spin ^{13}C in a methyl group could be estimated from the intensities of the ^{13}C multiplet components.

Introduction

It is well known that molecular motions prevail in biomolecules and they play a critical role in intermolecular interactions (Stites, 1997) and protein folding processes (Dyson and Wright, 1996; Onuchic et al., 1997). Among various biophysical methods, NMR provides site-specific dynamics information with the intrinsic nucleus probes (Kay and Petsko, 2001). With the advent of isotope-edited multidimensional NMR methods applied to a system consisting of ^{13}C-, ^{15}N-labeled protein, NMR spectroscopy becomes a powerful approach for quantifying molecular conformational dynamics at multiple atomic sites and over multiple time scales (Nesmelova et al., 2001; Palmer, 2001; Palmer et al., 1996). Up to now, most of the studies have been focused on the dynamics of backbone amides using ^{15}N relaxation times T_1 and T_2 and heteronuclear Overhauser effect (NOE) (Bruschweiler et al., 1995; Kay et al., 1989; Mandel et al., 1996; Mulder et al., 2000), as the ^{15}N relaxation data can be easily recorded and interpreted. In some cases, the protein backbone is found to be unaffected upon ligand binding, while on the contrary, dynamics of side chains is significantly perturbed (Constantine et al., 1998; Lee et al., 2000). In general, there is no direct correlation between main chain and side chain motions (Wand, 2001). In understanding protein structure-function relationship, it is also necessary to study the dynamics of side chains.

Carbon nuclei are located in both protein backbone and side chains. As such, ^{13}C relaxation should in principle offer a greater wealth of information on dynamics. For uniformly ^{13}C-labeled samples, methods have been developed to measure the auto-relaxation of $^{13}C_\alpha$ and ^{13}CO (Engelke and Ruterjans, 1995; Yamazaki et al., 1994) or cross-correlated relaxation between chemical shift anisotropy (CSA) and dipolar interactions (Fischer et al., 1997). But due to ^{13}C-^{13}C

*To whom correspondence should be addressed, E-mail: dbsydw@nus.edu.sg

J coupling and cross-correlated relaxation between ^{13}C-^{1}H dipoles, the application of ^{13}C relaxation is nevertheless greatly limited. A number of methods aiming to resolve the problem arising from $^{1}J_{CC}$ have since been used to extract information on dynamics from ^{13}C relaxation; these involve fractional ^{13}C enrichment (Wand et al., 1996), ^{13}C site-specific labeling (Lee et al., 1997; Nicholson et al., 1992) and the absence of ^{13}C enrichment (Palmer et al., 1991). However, for CH_2 and CH_3 systems, the data interpretation is still complicated by the dipolar cross-correlated relaxation. An experiment designed recently to solve both problems of J coupling and cross-correlated relaxation was done by choosing only C-H two-spin systems in a sample with alternating ^{13}C-^{12}C labeling patterns in concert with partial deuteration (LeMaster and Kushlan, 1996). Alternatively, the deuteron nucleus rather than carbon can be used as a probe for dynamics to avoid J coupling and cross-correlation problems. Kay's group recently developed a number of methods to study the dynamics of methyl and methylene groups (Millet et al., 2002; Muhandiram et al., 1995; Yang et al., 1998). However, application of methods based on special isotope labeling is limited by sample preparation and spectral resolution of 2D ^{13}C-^{1}H correlation maps.

Cross-correlated relaxation is recognized by the difference in line widths of the different multiplets in a two or more spin system known also as the interference effect (Goldman, 1984; Mayne et al., 1976). While it needs to be suppressed in the measurement of auto-correlated relaxation, its measurement alone is an alternative way of obtaining dynamics and structural information (Reif et al., 1997; Tjandra et al., 1996; Yang et al., 1997). In CH_2 and CH_3 systems, cross-correlation spectral density functions can be obtained from the measurements of initial relaxation times of the ^{13}C multiplets (Daragan and Mayo, 1993; Zheng et al., 1993). However the approach is restricted to only small molecules or specifically labeled macromolecules. A more practical method to detect the signal resulting from cross-correlated relaxation between dipoles was proposed by Ernst (Ernst and Ernst, 1994) and later improved by Rüterjans (Engelke and Rüterjans, 1998). Although the sign of the cross-correlation signal can be used to discriminate a restricted motional model from an unrestricted one, no quantitative information has been obtained to date. Recently, we developed a technique to measure the cross-correlated relaxation rate between C-H dipoles in a CH_2 group from the intensities of ^{13}C triplet components (Yang et al., 1998, 1999). Cross-correlation rates were well correlated to auto-correlation order parameters determined from deuterium relaxation of CHD groups (Yang et al., 1998). In comparison to the measurement of deuterium relaxation in CHD, cross-correlated relaxation can be more easily determined from a single 3D spectrum using a uniformly ^{13}C-, ^{15}N-labeled sample. In fact, a cross-correlation rate like order parameter reflects the degree of spatial restriction in the CH_2 group (Yang et al., 1998).

In order to study the dynamics of methyl groups in a uniformly ^{13}C-, ^{15}N-labeled sample, which is normally used for structural determination, we present here a novel approach on the basis of cross-correlated relaxation between C-H dipoles. The method is applied to study the methyl dynamics of human intestinal fatty acid binding protein in the absence of ligand.

Materials and methods

^{15}N, ^{13}C uniformly labeled IFABP was expressed and purified as described previously (Zhang et al., 1997). NMR experiments were performed on a sample of 1.0 mM protein, pH 7.0, 90% H_2O, 10% D_2O, and at 25 °C. All the experiments were recorded on a Bruker Avance DRX 500 MHz spectrometer equipped with pulse field gradient units and an actively shielded cryoprobe. To obtain the overall rotational correlation time of IFABP in the absence of fatty acid, ^{15}N relaxation times, T_1, $T_{1\rho}$ and heteronuclear NOEs were recorded. 3D experiments were performed for measuring cross-correlated relaxation using the pulse scheme described in Figure 1. 32 scans were accumulated for each point in the indirect dimensions using a relaxation delay of one second. The 3D data comprised of $82 \times 18 \times 512$ complex points with spectral widths of 3000, 1340 and 8000 Hz in ^{13}C, ^{15}N and ^{1}H dimensions, resulting in a total experimental time of 64 hours. The data was apodized with a sine weighting function shifted by 63° in the direct proton dimension. The ^{13}C and ^{15}N time domains were doubled by linear prediction prior to the application of a cosine-squared window function. After zero filling and Fourier transformation, the final data sets comprised of 1024, 128 and 1024 points along the F3, F2 and F1 dimensions, respectively. Processing of the spectra was carried out using NMRPipe software (Delaglio et al., 1995) and analyzed using Pipp-capp software (Garrett et al., 1991).

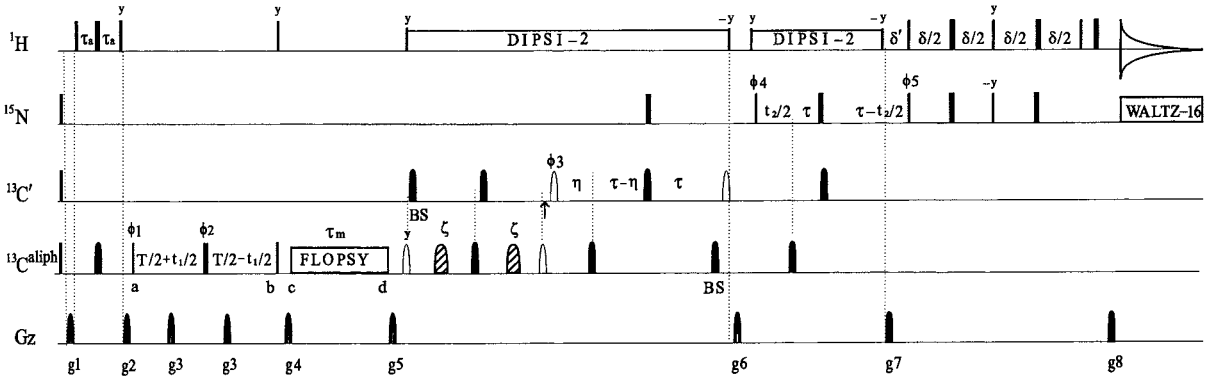

Figure 1. Pulse scheme for measuring the cross-correlated relaxation of methyl carbons. All narrow (wide) rectangular pulses are applied with a flip angle of 90° (180°). The carriers are centered at 4.7 and 119 ppm for ^{1}H and ^{15}N, respectively. The ^{13}C carrier is set at 40 ppm until immediately prior to the ^{13}C′ pulse of phase ϕ_3 at which time the carrier is jumped to 176 ppm. All ^{1}H pulses are applied using a 40 kHz field while the ^{13}C rectangular pulses are applied with a 19.2 kHz field. All the ^{13}C shaped 90° pulses (opened shaped) have a G4 profile (400 μs, 11.7 kHz peak rf, 9 kHz bandwidth). All the ^{13}C shaped 180° pulses (filled shaped) have a Q3 profile (Emsley and Bodenhausen, 1992) (300 μs, 11.0 kHz peak rf, 9 kHz bandwidth), except for the first and fourth shaped 180° pulses. The first ^{13}C shaped 180° pulse has a REBURP profile (Geen and Freeman, 1991) with a duration of 1.5 ms and excitation centered at 20 ppm (2.6 kHz bandwidth). The fourth $^{13}C^{aliph}$ shaped pulse is a 400 μs 180° REBURP shape with a maximum field of 15.6 kHz (10 kHz bandwidth). The ^{13}C shaped 180° pulses (shaded, 1.5 ms) applied in the middle of the delays ζ have an IBURP2 profile centered at 33 ppm with a band width of ±11 ppm. These refocus the $^{13}C_\alpha$-$^{13}C_\beta$ couplings for most of the residues. The ^{13}C spin-lock field strength for FLOPSY is 7 kHz. A decoupling power of 1 kHz is used during acquisition. Delays used are τ_a = 1.9 ms; T = 27.6 ms; τ_m = 21 ms; ζ = 3.8 ms; η = 4.5 ms; τ = 12.4 ms; δ′ = 5.4 ms; δ = 4.6 ms. The phase cycling used is: ϕ_1 = x, ϕ_2 = x, y, −x, −y; ϕ_3 = 2(x), 2(−x); ϕ_4 = 4(x), 4(−x); ϕ_5 = x, rec = x, −x, −x, x, −x, x, x, −x. Quadrature detection in the F1 dimension is achieved by State-TPPI of ϕ_1, while quadrature detection in F2 dimension uses the enhanced sensitivity pulse field gradient method (Kay et al., 1992b), where for each t_2 separate data sets are recorded for (g7,ϕ_5) and (−g7, ϕ_5 + 180°). For each successive t_2 value, ϕ_4 and the phase of the receiver are incremented by 180°. The duration and peak strengths of the sine-shaped gradients are: g1 = (1 ms, 20 G/cm); g2 = (2 ms, −30 G/cm); g3 = (0.2 ms, 40 G/cm); g4 = (4 ms, 25 G/cm); g5 = (1 ms, 25 G/cm); g6 = (0.5 ms, 20 G/cm); g7 = (1 ms, 40 G/cm); g8 = (1 ms, 4 G/cm).

Results and discussion

Pulse sequence for measuring methyl ^{13}C relaxation

Figure 1 illustrates the pulse scheme for measuring cross-correlated relaxation between ^{13}C-^{1}H dipoles and between ^{13}C-^{1}H dipole and CSA of the spin ^{13}C in CH_3 groups, using a uniformly ^{13}C-, ^{15}N-labeled protein sample. The pulse sequence is similar to the CC(CO)-NH TOCSY (total correlation spectroscopy) scheme (Montelione et al., 1992). The magnetization transfer is shown schematically as follows:

$$^{1}H \overset{J_{CH}}{\rightarrow} {}^{13}CH_3(CT\ t_1) \overset{J_{CC}}{\rightarrow} {}^{13}C_\alpha \overset{J_{C\alpha CO}}{\rightarrow}$$

$$^{13}CO \overset{J_{CON}}{\rightarrow} {}^{15}N\ (CT\ t_2) \overset{J_{NH}}{\rightarrow} NH\ (t_3),$$

where CT t_i is a constant-time acquisition period.

Magnetization originating from protons is transferred to their attached ^{13}C spin via INEPT. From point *a* to *b*, the ^{13}C quartet components are modulated by their own resonant frequencies and relaxation rates in a constant-time acquisition mode under free precession. At point *b*, the 90° proton pulse and subsequent gradient destroy magnetization other than C_z and C_zH_{ZQ}, where C_z and H_{ZQ} represent carbon longitudinal and proton zero-quantum magnetizations, respectively. During the period from point *c* to *d*, each of the quartet components is equally transferred to the $^{13}C_\alpha$ of the same amino acid residue via a FLOPSY (flip-flop spectroscopy) sequence. Thus, in the absence of cross-correlation during the CT t_1 period, evolution of C_yH_z magnetization under proton J coupling interaction results in quartet components with a 1:1:-1:-1 intensity ratio in the F1 dimension. This is extremely important, since cross-correlated relaxation rates are measured based on the relative intensities of the ^{13}C quartet. From the point *d* onwards, magnetization is transferred to the amide proton of the following residue for detection. The initial 90° pulses on ^{13}C followed by a pulse field gradient before the first proton pulse are applied in this experiment, which assure that the subsequent carbon magnetization is from a net polarization transfer from its attached protons.

Theory

For a reference on the evolution of the spin density operator – eigenfunctions, transitions and transition

frequencies in an isolated AX_3 spin system are given in the appendix of this paper, where notations used are similar to Kay's (Kay and Bull, 1992). For protons, there are ten transitions but two apparent resonant frequencies $\omega_X + \pi J_{AX}$ and $\omega_X - \pi J_{AX}$. For ^{13}C, there are eight transitions but four apparent resonant frequencies. The eight transitions can be recasted into the following: Four single-quantum coherences (M_1, M_2, M_4 and M_6) that are the observable quartet of spin A in the presence of J coupling with spins X, two multiple-quantum coherences (M_3 and M_5) and two unobservable coherences (M_7 and M_8). The ^{13}C quartet components at frequencies $\omega_A + 3\pi J_{AX}$, $\omega_A + \pi J_{AX}$, $\omega_A - \pi J_{AX}$ and $\omega_A - 3\pi J_{AX}$ are referred to as outer peak 1 ($M_1 = \rho_{1,9}$), inner peak 1 ($M_2 = (\rho_{2,10} + \rho_{5,13} + \rho_{7,15})/\sqrt{3}$), inner peak 2 ($M_4 = (\rho_{3,11} + \rho_{6,14} + \rho_{8,16})/\sqrt{3}$) and outer peak 2 ($M_6 = \rho_{4,12}$). Each of the two inner peaks consists of three degenerate transitions.

If we neglect proton relaxation during the first INEPT period, the magnetization at point *a* in the pulse sequence is C_yH_z, where C_y and H_z denotes y and z components of carbon and proton magnetization. This indicates that the four carbon resonances of a CH_3 group have an initial intensity ratio of 1:1:-1:-1. However, due to auto- and cross-correlated relaxations among ^1H_i - ^1H_j and ^1H_i - ^{13}C (i, j = 1, 2 and 3, and i $\neq$ j) dipolar interactions during the INEPT period, the initial intensity ratio of the ^{13}C quartet at point *a* may differ from 1:1:-1:-1. In order to evaluate such relaxation effects, we derived the origins of the carbon coherences at point *a* in Figure 1. Carbon coherences $\rho_{1,9}$, $\rho_{2,10}$, $\rho_{3,11}$ and $\rho_{4,12}$ arose as a result of transfers from proton transitions of the 3/2 manifold and $\rho_{5,13}$, $\rho_{6,14}$, $\rho_{7,15}$ and $\rho_{8,16}$ from proton transitions of the 1/2 manifold. At point *a*, the intensities of the outer and inner lines are

$$\begin{aligned} I_{\text{out1}}(0) &= 3/8(I_{\text{H1}} + I_{\text{H3}}) + 3/4 I_{\text{H2}} \\ &= 3/8[\exp(-R_{\text{H11}}2\tau_a) + \exp(-R_{\text{H33}}2\tau_a)] \\ &\quad + 3/4\exp(-R_{\text{H22}}2\tau_a), \end{aligned} \tag{1.1}$$

$$\begin{aligned} I_{\text{in1}}(0) &= 3/8(I_{\text{H1}} + I_{\text{H3}}) - 1/4 I_{\text{H2}} + I_{\text{H4}}/2 + I_{\text{H5}}/2 \\ &= 3/8[\exp(-R_{\text{H11}}2\tau_a) + \exp(-R_{\text{H33}}2\tau_a)] \\ &\quad - \exp(-R_{\text{H22}}2\tau_a)/4 + \exp(-R_{\text{H44}}2\tau_a)/2 \\ &\quad + \exp(-R_{\text{H55}}2\tau_a)/2, \end{aligned} \tag{1.2}$$

$$I_{\text{out2}}(0) = -I_{\text{out1}}(0), \tag{1.3}$$

$$I_{\text{in2}}(0) = -I_{\text{in1}}(0), \tag{1.4}$$

where I_{out1} and I_{out2} are the respective intensities of outer peak 1 and outer peak 2; I_{in1} and I_{in2} are the respective intensities of inner peak 1 and inner peak 2; I_{Hi} is the intensity of the i_{th} proton transition at the end of INEPT transfer and R_{Hii} is the proton relaxation matrix element, as given in appendix.

Since the proton transverse relaxation is dominated by spectral density function J(0), all other spectral densities at high frequencies were ignored in the calculation of proton relaxation. If a CH_3 group is rotating rapidly about its C_3 axis and is attached to a spherical molecule tumbling sufficiently slowly that only J(0) needs to be considered, the auto- and cross-correlation spectral densities are identical (Bull, 1992) ($J_{AX}(0) = J_{AX,AX}(0)$ and $J_{XX}(0) = J_{XX,XX}(0)$). In this case, the relaxations for all of the $1/2 \leftrightarrow -1/2$ transitions of the 3/2 and 1/2 manifolds are the same ($R_{\text{H44}} = R_{\text{H55}} = R_{\text{H22}}$). Thus, the intensities of the outer and inner lines become the same ($I_{\text{in1}} = I_{\text{out1}}$) based on eqs. 1.1 and 1.2. In contrast, the transfer of magnetization from carbon to proton is more complicated as shown by Kay et al. (1992a). Numerical simulations for various internal motions and overall correlation times (3–15 ns) indicated that the intensity difference between the ^{13}C inner and outer peaks was always less than 0.5% at point *a* in the pulse sequence. The intensities of the two multiple quantum coherences resulting from cross-correlated relaxation during the INEPT period were in the range of 0–45%, relative to single-quantum coherences. The inner/outer peak ratio is independent of the duration of τ_a. Therefore an initial intensity ratio of 1:1:-1:-1 can always be used for the four apparent resonances at the beginning of the ^{13}C relaxation period.

During the period from *a* to *b*, carbon coherences evolve under the modulations of resonance frequencies. At the same time, their decays are governed by auto- and cross-correlated relaxation resulting from dipolar and CSA interactions within the methyl group as well as dipole-dipole interactions among methyl protons and their proximal protons. The evolution of the ^{13}C coherences can be described as:

$$\frac{dM}{dt} = -\begin{bmatrix} i\omega_A + i3\pi J + R_{11} & R_{12} & R_{13} \\ R_{12} & i\omega_A + i\pi J + R_{22} & R_{23} \\ R_{13} & R_{23} & i\omega_A + i\pi J + R_{33} \\ R_{14} & R_{24} & R_{34} \\ R_{15} & R_{25} & R_{35} \\ R_{16} & R_{26} & R_{36} \end{bmatrix}$$

$$\begin{bmatrix} R_{14} & R_{15} & R_{16} \\ R_{24} & R_{25} & R_{26} \\ R_{34} & R_{35} & R_{36} \\ i\omega_A - i\pi J + R_{44} & R_{45} & R_{46} \\ R_{45} & i\omega_A - i\pi J + R_{55} & R_{56} \\ R_{46} & R_{56} & i\omega_A - i3\pi J + R_{66} \end{bmatrix} \bullet \begin{bmatrix} M_1 \\ M_2 \\ M_3 \\ M_4 \\ M_5 \\ M_6 \end{bmatrix}, \quad (2)$$

where **M** is a vector containing six coherences ($M_i, i = 1 - 6$); J is the scalar coupling constant between proton and carbon in the CH_3 group; R_{ij} is the ij_{th} relaxation matrix element as given in appendix. The two unobservable coherences M_7 and M_8 do not couple with other coherences. They are therefore not included in the differential equation.

Due to cross-correlated relaxation and proton-proton spin flips arising from protons surrounding the methyl group, off-diagonal elements in Equation 2 are not equal to zero and the magnetizations eventually decay in a multi-exponential manner. If the frequency difference between M_i and M_j is much larger than its cross-relaxation rate (i.e., $|\omega_{ii} - \omega_{jj}| >> R_{ij}$), R_{ij} can be neglected. In this case, the cross-relaxation R_{ij} has no effect on the decays of M_i and M_j. This is similar to Redfield's secular approximation (Bull, 1991; Redfield, 1957). Keeping this approximation in mind, we can see that the two outer lines M_1 and M_6 relax in a single exponential form. On the other hand, inner peaks M_2 and M_4 cross-relax with multiple-quantum coherences M_3 and M_5, respectively, and should thus be expected to display multi-exponential decays. The cross-relaxation rate R_{23} is governed by high frequency spectral densities $J(\omega_A + \omega_X)$, $J(\omega_A - \omega_X)$ and $J(\omega_X)$ while $R_{33} - R_{22}$ ($\approx 2R_{2H} - R_{1Hsel}$) is governed by the proton transverse relaxation rate. As such $R_{23} << R_{33} - R_{22}$ and $R_{45} << R_{55} - R_{44}$, for proteins with overall correlation times larger than 2 ns. Hence we can still describe the initial relaxation of M_2 and M_4 in a mono-exponential form during a short constant-time period of ~ 28 ms. This approximation is also confirmed by numerical simulations, as will be shown later.

At the end of the constant period (point *b* in the pulse sequence), the intensities of the four single-quantum coherences are:

$$\begin{aligned} I_{out1} = \exp[&-(3\Gamma_{AX} + 3\Gamma_{AX,AX} + 3\Gamma_{AX,A} \\ &+\Gamma_A + 6J_{XX}(2\omega_X) + 3J_{XX}(\omega_X) \\ &+3J_{XX,XX}(\omega_X) + 1.5R_{1Hsel})T], \end{aligned} \quad (3.1)$$

$$\begin{aligned} I_{out2} = -\exp[&-(3\Gamma_{AX} + 3\Gamma_{AX,AX} - 3\Gamma_{AX,A} \\ &+\Gamma_A + 6J_{XX}(2\omega_X) + 3J_{XX}(\omega_X) \\ &+3J_{XX,XX}(\omega_X) + 1.5R_{1Hsel})T], \end{aligned} \quad (3.2)$$

$$\begin{aligned} I_{in1} = \exp[&-(3\Gamma_{AX} - \Gamma_{AX,AX} + \Gamma_{AX,A} \\ &+\Gamma_A + 2J_{XX}(2\omega_X) + 3J_{XX}(\omega_X) \\ &-J_{XX,XX}(\omega_X) + 1.5R_{1Hsel})T], \end{aligned} \quad (3.3)$$

$$\begin{aligned} I_{in2} = -\exp[&-(3\Gamma_{AX} - \Gamma_{AX,AX} - \Gamma_{AX,A} \\ &+\Gamma_A + 2J_{XX}(2\omega_X) + 3J_{XX}(\omega_X) \\ &-J_{XX,XX}(\omega_X) + 1.5R_{1Hsel})T], \end{aligned} \quad (3.4)$$

where Γ_{AX} and Γ_A are auto-relaxation rates resulting from A-X dipole and CSA interactions respectively; R_{1Hsel} is the spin flip-flop rate of methyl protons; $\Gamma_{AX,AX}$ and $\Gamma_{AX,A}$ are cross-correlated relaxation between dipoles $A\text{-}X_i$ and $A\text{-}X_j$ and between dipole A-X and CSA of spin A, respectively; T is the duration of the constant-time period.

$$\Gamma_{AX,AX} = 4/3J_{AX,AX}(0) + J_{AX,AX}(\omega_A), \quad (3.5)$$

$$\Gamma_{AX,A} = 4/3J_{AX,A}(0) + J_{AX,A}(\omega_A), \quad (3.6)$$

where $J(\omega)$ is spectral density function as shown in Appendix A.

Using the intensities of the quartet, we can obtain the following relaxation rate:

$$\Gamma = \ln[I_{in1}I_{in2}/(I_{out1}I_{out2})]/(8T) \quad (4.1)$$

$$= \Gamma_{AX,AX} + J_{XX}(2\omega_X) + J_{XX,XX}(\omega_X). \quad (4.2)$$

In addition to the above, we also obtain cross-correlated relaxation rate between the dipole and CSA interaction:

$$\Gamma_{AX,A} = \ln[-I_{out2}/I_{out1}]/(6T) = \ln[-I_{in2}/I_{in1}]/(2T). \quad (5)$$

$\Gamma_{AX,A}$ may also be measured from the two inner peaks, but the experimental error could be larger than that obtained from the two outer lines since the relaxation rate difference between the inner lines is one-third as large as that between the two outer lines.

Justification of dipole-dipole cross-correlation rate measured from peak intensities through numberical simulations

To assess how much error can be introduced, by assuming each of the ^{13}C quartet components decays in a single-exponential form, we solved Equation 2 numerically and obtained the intensities of the four single-quantum magnetizations at point *b* in the pulse sequence. The resultant intensities were used to calculate an actual rate Γ' that corresponds to the rate measured experimentally using Equation 4.1. The errors were established by comparing Γ' and Γ that was calculated according to Equation 4.2. In the simulation, relaxation matrix elements were calculated using equations shown in the appendix, assuming a C-H bond length of 1.09 Å, an axially symmetric ^{13}C CSA of 25 ppm with its symmetric axis coincident with the C_3 axis and an ideal tetrahedral geometry for methyl groups. Various overall correlation times (3–15 ns) and internal motions ($S_{axis}{}^2 = 0.1 - 1$, $\tau_{axis} = 50 - 500$ps, $\tau_f = 5 - 100$ps) were considered. The proton spin flip-flop rate R_{1Hsel} contributes to some of the off-diagonal elements of the relaxation matrix and thus causes error in the measurement of $\Gamma_{AX,AX}$ using Equation 4.1. Hence proper R_{1Hsel} values should be used in the simulations. Methyl protons interact with many surrounding protons with unknown internal motions and it would be very difficult to calculate proton spin flip-flop rate R_{1Hsel} and proton transverse relaxation rate R_{2H} arising from proton-proton interactions. Experimentally, we can estimate R_{1Hsel} by measuring the relaxation rates of two-spin C_zH_z and single-spin C_z coherences. For human intestinal fatty acid binding protein, we found that R_{1Hsel} varied from 3.5 to 10 s^{-1} at 25 °C. Although there was a correlation between the values of R_{1Hsel} and methyl dynamics ($S_{axis}{}^2$, which was estimated from cross-correlated relaxation rates), several methyl groups have nearly the same R_{1Hsel} values while their $S_{axis}{}^2$ values differ by a factor of 1.5. For error estimation purpose, we can take the largest R_{1Hsel} as the methyl proton spin flip rate of all the residues in human IFABP, which will result in an error overestimation. Unlike non-selective longitudinal relaxation rate (R_1) that contains no J(0) term, the selective proton longitudinal relaxation rate (R_{1Hsel}) is dominated by J(0). It can be approximated as $R_{1Hsel} = c^*\tau_m$, where c is a constant. According to the maximum value of R_{1Hsel} (10 s^{-1}) and τ_m (8.4 ns) for IFABP, the constant c was estimated to be 10/8.4 (s^{-1}/ns). Proton transverse relaxation R_{2H} is dominated by J(0) and is about 2.5 times as large as R_{1Hsel}. In our simulations, we simply assumed that $R_{1Hsel} = 10^*\tau_m/8.4$ and $R_{2H} = 2.5^*R_{1Hsel}$ for various sizes of proteins. For proteins, the average coupling constant for CH_3 groups is about 127 Hz with a standard deviation of 3 Hz and thus a constant-time of 27.6 ms is used in the experiment. The constant-time T simultaneously satisfies that $2\pi J_{CH}T \approx n\pi$ and $\pi J_{CC}T \approx \pi$, where n is an integer number and Jcc is the one-bond scalar coupling constant between carbons. When $2\pi J_{CH}T = n\pi$, the error arising from the assumption of single-exponential relaxation is always less than 0.05 s^{-1} ($|\Gamma' - \Gamma| < 0.05$ s^{-1}). When $2\pi JT \neq n\pi$ and the side chain motions are restricted, the error can be significantly larger than 0.05 s^{-1} since the spin flip-flop effect can not be averaged out to zero (Ghose and Prestegard, 1998). Figure 2 shows the fractional error $(\Gamma' - \Gamma)/\Gamma$ when $\tau_f = 50$ ps, $\tau_s = 150$ ps, J = 130 Hz and T = 27.6 ms. The small fractional errors indicate that the rate Γ measured from peak intensities approximately equals $\Gamma_{AX,AX} + J_{XX}(2\omega_X) + J_{XX,XX}(\omega_X)$. Below we will show that $\Gamma_{AX,AX} \approx \ln[I_{in1}I_{in2}/(I_{out1}I_{out2})]/(8T)$:

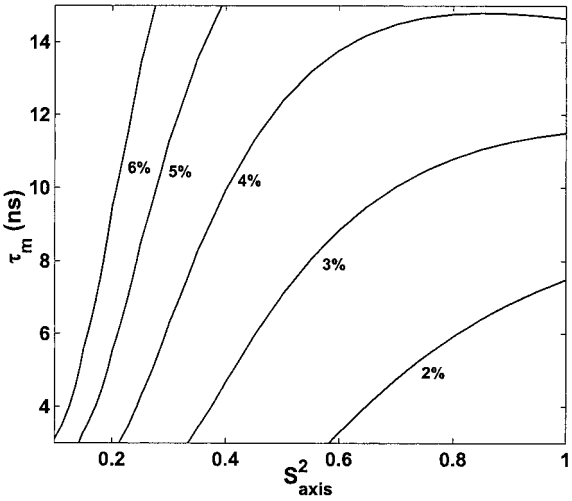

Figure 2. Comparison of Γ' and Γ when $\tau_f = 50$ ps, $\tau_s = 150$ ps, J = 130 Hz and T = 27.6 ms. The contours show the dependence of the fractional error $(\Gamma' - \Gamma)/\Gamma^*100$ on τ_m and S^2_{axis}. Γ' was calculated according to Equation 4.1 where the intensities were obtained by solving Equation 2 numerically. Γ was calculated according to Equation 4.2.

$J_{XX}(2\omega_X)$ and $J_{XX,XX}(\omega_X)$ are normally much smaller than $J_{AX,AX}(0)$ and $J_{AX,AX}(\omega_A)$. For various correlation times (3–15 ns) and internal motions ($S_{axis}{}^2 = 0.1-1$, $\tau_{axis} = 100$–500 ps, $\tau_f = 5$–100 ps), we found that the value of $J_{XX}(2\omega_X) + J_{XX,XX}(\omega_X)$

increases with decrease of $S_{axis}{}^2$ but is always less than 0.4 s^{-1} at a proton frequency of 500 MHz. At higher fields, it is even smaller (< 0.2 s^{-1} on an 800 MHz spectrometer). Therefore, Γ can be approximated as $\Gamma_{AX,AX}$ in its application to dynamics of medium size proteins. For very flexible methyl groups ($S_{axis}{}^2 < 0.3$) however, the cross-correlation rates are small and the contribution of $J_{XX}(2\omega_X)+J_{XX,XX}(\omega_X)$ to Γ could be more than 10%.

As shown in Figure 1, magnetization is transferred from methyl to NH of the subsequent residue. It is important to establish if the quartet components are transferred in an equal manner during the TOCSY period. At point *c* in the sequence, each component corresponds to coherence $C_Z[1 + c^*H_{ZQ}]$, where c is a constant and its value varies for inner to outer lines. In the absence of the H_{ZQ} term, all of the quartet components are transferred equally to C_Z^α during the FLOPSY period and further to NH to be detected. C_ZH_{ZQ} may be transferred to C_Z first via cross-correlation effect and then to C_Z^α through TOCSY process. Fortunately, the cross-relaxation rate between C_Z and C_ZH_{ZQ} is very small (< 0.5 s^{-1}) (Bull, 1992). Within a duration of 21 ms, the net transfer from C_ZH_{ZQ} to C_Z and then to C_Z^α is negligible as established from simulations. Therefore, cross-correlated relaxation rates between dipole-dipole and dipole-CSA in CH_3 groups can be measured using the scheme shown in Figure 1.

Software availability

The computer program used to simulate Γ and S'^2 was written in MATLAB language. It is available from the authors upon request.

Evaluation of $^{13}CH_3$ CSA values

The magnitude of the $^{13}CH_3$ CSA is assumed to be 25 ppm in relaxation data analysis. It can actually be estimated from cross-correlated relaxation rate $\Gamma_{AX,A}$, based on Equation 3.6, provided that the motional parameters and model are known for a methyl group. Alternatively, it can be obtained in a manner independent of motional parameters, using the ratio of $\Gamma_{AX,A}/\Gamma_{AX,AX}$ based on Equations 3.5–3.6. Assuming the symmetric axis of the CSA tensor is the same as the rotational axis of methyl group, in the case of $S_{axis}{}^2 > 0.3$ and $\tau_m > 3$ ns, the magnitude of the ^{13}C CSA is given to excellent approximation by:

$$\sigma_\parallel - \sigma_\perp = -\tfrac{2}{3}(\mu_0 h/8\pi^2\gamma_A\gamma_X/r_{AX}{}^3)/\omega_A \ln[-I_{out2}/I_{out1}]/\ln[I_{in1}I_{in2}/(I_{out1}I_{out2})]. \quad (6)$$

When the methyl group is highly flexible, e.g., $S_{axis}{}^2 < 0.3$, it becomes difficult to accurately measure the magnitude of the CSA tensor due to the significant contribution of $J_{XX}(2\omega_X) + J_{XX,XX}(\omega_X)$ to Γ.

Application to intestinal fatty acid binding protein

The method developed above for the measurements of cross-correlated relaxation rates of methyl groups was applied to study the methyl dynamics of human apo-IFABP with uniformly ^{13}C-, ^{15}N-labeled protein. Figure 3a shows a number of F_1 slices from the 3D spectra, illustrating the ^{13}C multiplet components of residues A32, V118, I127γ and I27δ. As shown earlier, the difference in intensities of the quartet components are the result of cross-correlation between dipole-dipole and dipole-CSA relaxation interactions. The more restricted the motion of the methyl symmetric axis, the more deviation there is from a 1:1:-1:-1 intensity pattern.

A relaxation rate (Γ) which can be approximated as dipole-dipole cross-correlation rate ($\Gamma_{AX,AX}$) and a dipole-CSA cross-correlated relaxation rate ($\Gamma_{AX,A}$) can be derived from the intensity profiles. 33 out of 46 residues having methyl groups were measured. For some valine and leucine residues, the two methyl groups have degenerate ^{13}C chemical shifts. Thus only an average relaxation value can be obtained. The methyl groups in two methionine residues cannot be detected since the methyl carbon does not directly bond to a carbon and no TOCSY transfer occurs. The resonances of 6 residues had insufficient S/N for the reliable measurement of the intensities of multiplet components. Spectral overlap was found for several Val and Leu residues. This can occur when the chemical shift difference between the geminal methyl ^{13}Cs in Val and Leu is close to $^1J_{CH}$, 2^1J_{CH}, or 3^1J_{CH}. In total, we obtained relaxation data for 45 (out of 74) methyl. Figure 3b shows the resultant rates against residue number. The values of Γ distribute in the range of 1.3–6.9 s^{-1}, reflecting a dynamic variety of methyl groups located at various environment. The absolute values of $\Gamma_{AX,A}$ are much smaller than Γ since the dipole-CSA interaction is weaker than the dipole-dipole interaction and they are prone to experimental errors (data not shown).

Nevertheless, using the intensities of ^{13}C multiplet components, we can estimate the amplitudes of the $^{13}CH_3$ CSA tensors from Equation 6, assuming the axially symmetric axis of the CSA tensor is coincid-

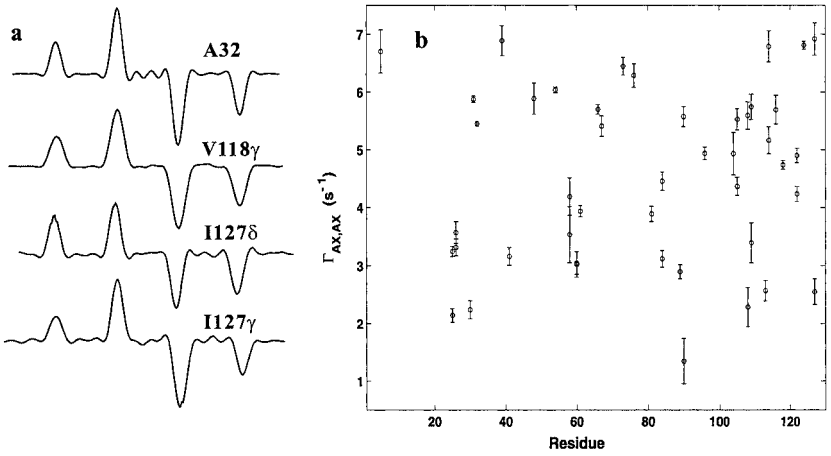

Figure 3. F1 $^{13}CH_3$ cross-section from data recorded on the IFABP sample that are uniformly labeled with ^{13}C and ^{15}N (a). Each multiplet is split into a quartet from the one-bond scalar coupling. Due to dipole-dipole and dipole-CSA cross-correlated relaxation interactions, the intensity ratio deviates from 1:1:-1:-1. Dipole-dipole cross correlated relaxation rates derived from the intensities of the multiplets are plotted against residue number (b).

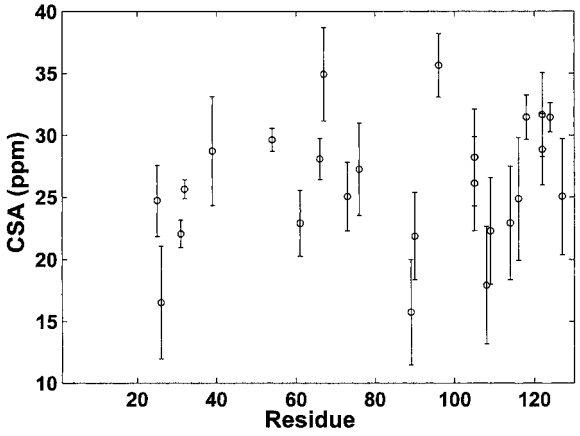

Figure 4. The magnitudes of methyl ^{13}C CSA tensor derived from the intensities of ^{13}C multiplets.

ent with the C_3 axis of the methyl group. Some of the resultant CSA values had large uncertainties due to insufficient signal to noise ratio. 25 CSA values with uncertainties less than 5 ppm were obtained. The CSA amplitudes distribute around 26.0 ppm with a standard deviation of 5.1 ppm as shown in Figure 4. The actual CSA amplitudes may deviate from the values shown here because the CSA tensor can be non-axially symmetric. Nevertheless, the average value and variations are consistent with previous studies using solid state NMR techniques (Ishima et al., 2001; Ye et al., 1993).

The value of Γ depends on both methyl dynamics and overall rotational correlation time. In order to obtain the dynamics, we can normalize Γ value using the following expression:

$$S'^2 = \Gamma / \Gamma_{max}, \quad (7)$$

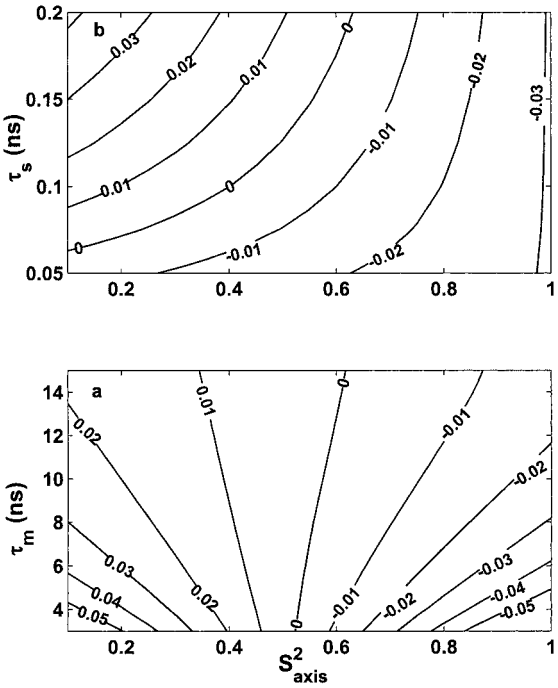

Figure 5. Comparison of S'^2 and ${S_{axis}}^2$. The contours show the dependence of the differences ($S'^2 - {S_{axis}}^2$) on τ_m and ${S_{axis}}^2$ when $\tau_f = 50$ ps, $\tau_s = 150$ ps, J = 127 Hz and T = 27.6 ms (a) and the dependence on τ_{axis} and ${S_{axis}}^2$ when $\tau_f = 50$ ps, $\tau_m = 8$ ns, J = 127 Hz and T = 27.6 ms (b).

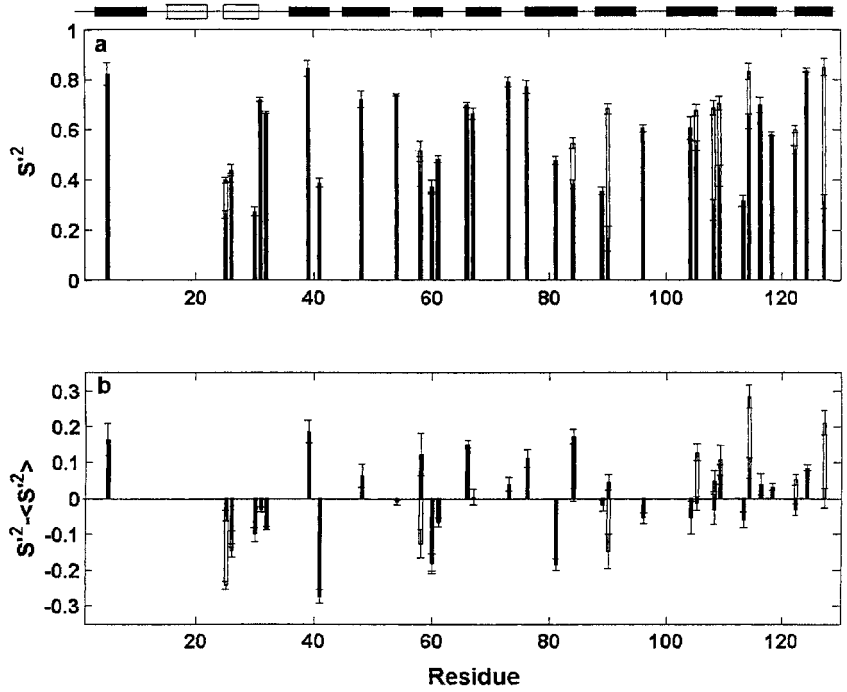

Figure 6. Normalized cross correlation rate (S'^2), which can be considered to be $S_{axis}{}^2$ that describes the degree of spatial restriction in the symmetrical axis of methyl (a). For the residues having two methyl groups (Ile, Leu, and Val), one is indicated by black bar while the other one by white bar. Differences between S'^2 and the average of S'^2 for each methyl type, $\langle S'^2 \rangle$, for methyls of IFABP in the absence of fatty acid (b). The top panel shows secondary structures, indicated with boxes (α-helices) or filled boxes (β-sheets).

where Γ_{max} is the value of Γ when there are no internal motions except rapid rotation about the C_3 axis ($\tau_{axis} = \infty$ and $\tau_f = 0$). When $\tau_m \geq 4$ ns, $\tau_{axis} = 50$–200 ps, $\tau_f = 5$–50 ps and $S_{axis}{}^2 > 0.25$, simulations indicated that S'^2 deviates from $S_{axis}{}^2$ by less than 0.1. The deviation increases with the increase of τ_{axis}. For most methyl groups (Constantine et al., 1998; Kay et al., 1996; Wand et al., 1996), the internal motional correlation time τ_{axis} is less than 200 ps. When $S_{axis}{}^2$ is small, S'^2 is larger than $S_{axis}{}^2$ because of the contribution of $J_{XX}(\omega_X)$ and $J_{XX,XX}(\omega_X)$ to Γ. When $S_{axis}{}^2$ is large, S'^2 is smaller than $S_{axis}{}^2$ because of the negative contribution of fast rotation (the second term in the spectral density function) to Γ. Figure 5a shows a contour plot of the differences ($S'^2 - S_{axis}{}^2$) when $\tau_f = 50$ ps, $\tau_s = 150$ ps, J = 127 Hz and T = 27.6 ms. When J = 130 Hz, the difference is still less than 0.06. Figure 5b shows a contour plot of the differences when $\tau_f = 50$ ps, $\tau_m = 8$ ns, J = 127 Hz and T = 27.6 ms. From the figure, we can see that the order parameter (S'^2) derived from Equation 7 should be reliable within an error of ±0.04 for IFABP when $S_{axis}{}^2 > 0.1$. In general, S'^2 can be approximated as $S_{axis}{}^2$ provided that methyl group is not highly flexible.

Using an overall correlation time 8.4 ns obtained from ^{15}N relaxation times at 25 °C, we calculated the values of S'^2 as shown in Figure 6a. The values of S'^2 range from 0.16 to 0.85. The large distribution of order parameters shown here is consistent with the conclusion drawn from methyl ^2H and ^{13}C relaxation studies, but is distinct from the S^2 values measured at backbone atoms, which range from 0.75 to 0.95 for most residues in regions with regular secondary structures. Although we did not measure S^2_{axis} values of the IFABP sample using ^2H relaxation, the data of its homologue (human muscle fatty acid binding protein, MFABP) in the absence of fatty acid are available (Constantine et al., 1998). Human IFABP and MFABP have relatively high sequence homology (73 out of 131 residues are positively matched between the two protein sequences, Blast E-value = 10^{-14}) and have similar tertiary structures. There are a number of methyl-containing residues that are conserved in both sequence and structure. The axis order parameters of these conserved residues available for both proteins are: 0.79, 0.35, 0.42, 0.70, 0.31 for A73, L89δ, I109δ, I109γ, L113δ of human IFABP and 0.83, 0.34, 0.40, 0.76, 0.25, 0.27 for A75, L91δ, I109δ, I109γ, L113δ1,

L113δ2 of MFABP (Constantine et al., 1998). We can see that the results obtained from cross-correlated relaxation agree very well with those measured from ^{2}H relaxation.

Unlike S^2 values measured at backbone atoms, order parameters at side chain atoms are position dependent. On average, the more distant the methyl group is from the backbone, the lower the S^2_{axis} value is, i.e., $S^2_{axis}(\beta) > S^2_{axis}(\gamma) > S^2_{axis}(\delta)$. To correct for the effect of position, averages of the S'^2 values for each methyl type, $\langle S'^2 \rangle$, were calculated. The differences between S'^2 and the appropriate $\langle S'^2 \rangle$ are shown in Figure 6b. S'^2 values in C-terminal part are higher than average, while many S'^2 values in methyl groups that are relatively isolated are lower than average. The residues located in the second helix (I25, V26, L30, A31 and A32) display lower order parameters than average in the absence of fatty acid. This is consistent with structural changes in solution, i.e., the binding of oleate to IFABP increases the helical content of the second α-helix and the order of the highly flexible ligand entry portal (Hodsdon and Cistola, 1997).

Conclusion

In the past, dipolar cross-correlated relaxation limited the application of ^{13}C relaxation data (T_1, T_2 and NOE) to studies on dynamics of CH_2 and CH_3 groups. Although isotope labeling techniques allowed one to probe into protein side chain dynamics, applications are still limited by additional sample preparation and spectral resolution of the C-H correlation map. The experiment shown here provides one with a simple solution to obtain data on side chain dynamics by using the same sample as in structural determination (uniformly ^{13}C-, ^{15}N-labeled proteins). With the availability of cryo-probe technology, this experiment is sufficiently sensitive to obtain statistically meaningful data for proteins with overall correlation times less than 10 ns. For a given protein, cross-correlated relaxation is dominated by motional amplitude of methyl groups, i.e., ${S_{axis}}^2$. Thus, the values of Γ alone or the order parameter S'^2 derived from Γ provide a rough quantitative description of methyl flexibility. In combination with T_1 and NOE, dynamic parameters (${S_{axis}}^2$, τ_{axis} and τ_f) can be determined more accurately, especially for very flexible residues and small sized proteins ($\tau_m < 4$ ns), where the contribution of $J_{XX}(2\omega_X) + J_{XX,XX}(\omega_X)$ cannot be ignored. Unlike transverse relaxation time T_2, which is complicated by conformational exchange, cross-correlated relaxation is free of chemical exchange and provides more reliable information on the dynamics of methyl groups.

Acknowledgements

This research has been supported by the National University of Singapore. We are grateful to Professors Lewis E. Kay and Kalpathy R. K. Easwaran for their critical evaluation of the manuscript. We thank Ms Ler Peggy for proofreading. Liu Weidong is a recipient of the National Science and Technology Board (now A*Star), Singapore research fellowship.

Appendix A

Eigenstates, proton and carbon transitions, and transverse relaxation matrices of spins A and X in an AX_3 spin system.

The first spin state in wavefunction |k > corresponds to the ^{13}C spin state and the remaining spin states are associated with the proton spins.

Eigenstates

$|1 >= \beta\alpha\alpha\alpha$ $|2 >= \beta(\alpha\alpha\beta + \alpha\beta\alpha + \beta\alpha\alpha)/\sqrt{3}$

$|3 >= \beta(\alpha\beta\beta + \beta\alpha\beta + \beta\beta\alpha)/\sqrt{3}$ $|4 >= \beta\beta\beta\beta$

$|5 >= \beta\alpha(\alpha\beta - \beta\alpha)\sqrt{2}$ $|6 >= \beta\beta(\alpha\beta - \beta\alpha)\sqrt{2}$

$|7 >= \beta(\alpha\alpha\beta + \alpha\beta\alpha - 2\beta\alpha\alpha)/\sqrt{6}$ $|8 >= \beta(\beta\beta\alpha + \beta\alpha\beta - 2\alpha\beta\beta)/\sqrt{6}$

$|9 >= \alpha\alpha\alpha\alpha$ $|10 >= \alpha(\alpha\alpha\beta + \alpha\beta\alpha + \beta\alpha\alpha)/\sqrt{3}$

$|11 >= \alpha(\alpha\beta\beta + \beta\alpha\beta + \beta\beta\alpha)/\sqrt{3}$ $|12 >= \alpha\beta\beta\beta$

$|13 >= \alpha\alpha(\alpha\beta - \beta\alpha)/\sqrt{2}$ $|14 >= \alpha\beta(\alpha\beta - \beta\alpha)/\sqrt{2}$

$|15 >= \alpha(\alpha\alpha\beta + \alpha\beta\alpha - 2\beta\alpha\alpha)/\sqrt{6}$ $|16 >= \alpha(\beta\beta\alpha + \beta\alpha\beta - 2\alpha\beta\beta)/\sqrt{6}$

Transitions and frequencies for spin X

$M_{H1} = \rho_{2,1}$ $\omega_{H1} = \omega_H - \pi J_{AX}$

$M_{H2} = \rho_{3,2}$ $\omega_{H2} = \omega_H - \pi J_{AX}$

$M_{H3} = \rho_{4,3}$ $\omega_{H3} = \omega_H - \pi J_{AX}$

$M_{H4} = \rho_{6,5}$ $\omega_{H4} = \omega_H - \pi J_{AX}$

$M_{H5} = \rho_{8,7}$ $\omega_{H5} = \omega_H - \pi J_{AX}$

$M_{H6} = \rho_{10,9}$ $\omega_{H6} = \omega_H + \pi J_{AX}$

$M_{H7} = \rho_{11,10}$ $\omega_{H7} = \omega_H + \pi J_{AX}$

$M_{H8} = \rho_{12,11}$ $\omega_{H7} = \omega_H + \pi J_{AX}$

$M_{H9} = \rho_{14,13}$ $\omega_{H9} = \omega_H + \pi J_{AX}$

$M_{H10} = \rho_{16,15}$ $\omega_{H10} = \omega_H + \pi J_{AX}$

Transitions and frequencies for spin A

$M_1 = \rho_{1,9}$ $\omega_1 = \omega_A + 3\pi J_{AX}$

$M_2 = (\rho_{2,10} + \rho_{5,13} + \rho_{7,15})/\sqrt{3}$ $\omega_2 = \omega_A + \pi J_{AX}$

$M_3 = (2\rho_{2,10} - \rho_{5,13} - \rho_{7,15})/\sqrt{6}$ $\omega_3 = \omega_A + \pi J_{AX}$

$M_4 = (\rho_{3,11} + \rho_{6,14} + \rho_{8,16})/\sqrt{3}$ $\omega_4 = \omega_A - \pi J_{AX}$

$M_5 = (2\rho_{3,11} - \rho_{6,14} - \rho_{8,16})/\sqrt{6}$ $\omega_5 = \omega_A - \pi J_{AX}$

$M_6 = \rho_{4,12}$ $\omega_6 = \omega_A - 3\pi J_{AX}$

$M_7 = (\rho_{5,13} - \rho_{7,15})/\sqrt{2}$ $\omega_7 = \omega_A + \pi J_{AX}$

$M_8 = (\rho_{6,14} - \rho_{8,16})/\sqrt{2}$ $\omega_8 = \omega_A - \pi J_{AX}$,

where J_{AX} is the scalar coupling constant between spins A and X; ω_H and ω_A are the Larmor frequencies of spin X and A, respectively.

Transverse relaxation matrix elements for spin X

$R_{H11} = 2/3J_{AX}(0) + 3J_{XX}(0) + 3J_{XX,XX}(0) + 16/3J_{AX,XX}(0)$

$R_{H22} = 10/9J_{AX}(0) - 4/9J_{AX,AX}(0) + 2J_{XX}(0) - 2J_{XX,XX}(0)$

$R_{H24} = -4/9J_{AX}(0) + 4/9J_{AX,AX}(0) + J_{XX}(0) - J_{XX,XX}(0)$

$R_{H25} = -R_{H24}$

$R_{H33} = 2/3J_{AX}(0) + 3J_{XX}(0) + 3J_{XX,XX}(0) - 16/3J_{AX,XX}(0)$

$R_{H44} = 4/3J_{AX}(0) - 2/3J_{AX,AX}(0) + J_{XX}(0) - J_{XX,XX}(0)$

$R_{H45} = -2/9J_{AX}(0) + 2/9J_{AX,AX}(0)$

$R_{H55} = R_{H44}$

$R_{Hij} = R_{Hji}$

$R_{H66} = R_{H33}\ R_{H77} = R_{H22}\ R_{H79} = R_{H24}\ R_{H710} = R_{H25}$

$R_{H88} = R_{H11}\ R_{H99} = R_{H44}\ R_{H910} = R_{H45}\ R_{H1010} = R_{H55}$

Only non-zero elements are shown above.

Transverse relaxation matrix elements for spin A

$R_{11} = 3\Gamma_{AX} + 3\Gamma_{AX,AX} + 3\Gamma_{AX,A} + \Gamma_A + 6J_{XX}(2\omega_X) + 3J_{XX}(\omega_X) + 3J_{XX,XX}(\omega_X) + 1.5R_{1Hsel}$

$R_{12} = \sqrt{3}[0.5J_{AX}(\omega_X) - J_{XX}(\omega_X) - J_{XX,XX}(\omega_X) - 0.5R_{1Hsel}]$

$R_{13} = 0.5\sqrt{6}[J_{AX,AX}(\omega_X) - J_{XX}(\omega_X) - 3J_{XX,XX}(\omega_X)]$

$R_{14} = -2\sqrt{3}J_{XX}(2\omega_X)$

$R_{15} = -2\sqrt{6}J_{XX,XX}(2\omega_X)$

$R_{16} = 0$

$R_{22} = 3\Gamma_{AX} - \Gamma_{AX,AX} + \Gamma_{AX,A} + \Gamma_A + 2J_{XX}(2\omega_X) + 3J_{XX}(\omega_X) - J_{XX,XX}(\omega_X) + 1.5R_{1Hsel}$

$R_{23} = \sqrt{2}[J_{AX,AX}(\omega_X) + 2J_{AX,AX}(\omega_A + \omega_X) + J_{AX,AX}(\omega_A - \omega_X)/3 + J_{XX}(\omega_X) + J_{XX,XX}(\omega_X) + 2J_{XX,XX}(2\omega_X)]$

$R_{24} = J_{AX,AX}(\omega_X) - 2[J_{XX}(\omega_X) - J_{XX,XX}(\omega_X)] - R_{1Hsel}$

$R_{25} = 0.5\sqrt{2}[J_{AX,AX}(\omega_X) - [J_{XX}(\omega_X) - J_{XX,XX}(\omega_X)]]$

$R_{26} = R_{14}$

$R_{33} = 3\Gamma_{AX} - \Gamma_{AX,AX} + \Gamma_{AX,A} + \Gamma_A + 4/3[J_{AX,AX}(0) - J_{AX}(0)] + 3[J_{XX}(0) - J_{XX,XX}(0)] + J_{AX,AX}(\omega_X) +$
$J_{AX,AX}(\omega_A - \omega_X)/3 +$
$2J_{AX,AX}(\omega_A + \omega_X) + 4J_{XX}(\omega_X) + 2J_{XX}(2\omega_X) + 2J_{XX,XX}(2\omega_X) + 0.5R_{1Hsel} + 2R_{2H}$

$R_{34} = R_{25}$

$R_{35} = 0.5J_{AX}(\omega_X) + J_{AX,AX}(\omega_X) - 2J_{XX,XX}(\omega_X) + 2J_{XX}(\omega_X)] - 0.5R_{1Hsel}$

$R_{36} = R_{15}$

$R_{44} = 3\Gamma_{AX} - \Gamma_{AX,AX} - \Gamma_{AX,A} + \Gamma_A + 2J_{XX}(2\omega_X) + 3J_{XX}(\omega_X) - J_{XX,XX}(\omega_X) + 1.5R_{1Hsel}$

$R_{45} = R_{23}$

$R_{46} = R_{12}$

$R_{55} = 3\Gamma_{AX} - \Gamma_{AX,AX} - \Gamma_{AX,A} + \Gamma_A + 4/3[J_{AX,AX}(0) - J_{AX}(0)] + 3[J_{XX}(0) - J_{XX,XX}(0)] + J_{AX,AX}(\omega_X) +$
$J_{AX,AX}(\omega_A - \omega_X)/3 +$
$2J_{AX,AX}(\omega_A + \omega_X) + 4J_{XX}(\omega_X) + 2J_{XX}(2\omega_X) + 2J_{XX,XX}(2\omega_X) + 0.5R_{1Hsel} + 2R_{2H}$

$R_{56} = R_{13}$

$R_{66} = 3\Gamma_{AX} + 3\Gamma_{AX,AX} - 3\Gamma_{AX,A} + \Gamma_A + 6J_{XX}(2\omega_X) + 3J_{XX}(\omega_X) + 3J_{XX,XX}(\omega_X) + 1.5R_{1Hsel}$

$$R_{ij} = R_{ji}$$
$$\Gamma_{AX} = 2/3J_{AX}(0) + 1/6J_{AX}(\omega_A - \omega_X) + 1/2J_{AX}(\omega_A) + 1/2J_{AX}(\omega_X) + J_{AX}(\omega_A + \omega_X)$$
$$\Gamma_{AX,AX} = 4/3J_{AX,AX}(0) + J_{AX,AX}(\omega_A)$$
$$\Gamma_{AX,A} = 4/3J_{AX,A}(0) + J_{AX,A}(\omega_A)$$
$$\Gamma_{A} = 4/3J_{AA}(0) + J_{AA}(\omega_A)$$
$$J_{AA}(\omega) = 1/15[\omega_i(\sigma_\parallel - \sigma_\perp)]^2\{{S_{axis}}^2\tau_m/[1 + (\omega\tau_m)^2] + (1 - {S_{axis}}^2)\tau_2/[1 + (\omega\tau_2)^2]\}$$
$$J_{ij,kl}(\omega) = 0.3(\mu_0 h/8\pi^2\gamma_i\gamma_j/{r_{ij}}^3)(\mu_0 h/8\pi^2\gamma_k\gamma_l/{r_{kl}}^3)j_{ij,kl}(\omega)$$
$$J_{ij}(\omega) = J_{ij,ij}(\omega)$$
$$J_{ij,i}(\omega) = 0.2(\mu_0 h/8\pi^2\gamma_i\gamma_j/{r_{ij}}^3)\omega_i(\sigma_\parallel - \sigma_\perp)j_{ij,i}(\omega)$$
$$j_{ij,kl}(\omega) = S^2\tau_m/[1 + (\omega\tau_m)^2] + [P_2(\boldsymbol{\mu_{ij}} \cdot \boldsymbol{\mu_{kl}}) - {S_f}^2]\tau_1/[1 + (\omega\tau_1)^2] + {S_f}^2(1 - {S_{axis}}^2)\tau_2/[1 + (\omega\tau_2)^2]$$
$$j_{ij,i}(\omega) = S^2\tau_m/[1 + (\omega\tau_m)^2] + [P_2(\boldsymbol{\mu_{ij}} \cdot \boldsymbol{\mu_i}) - {S_f}^2]\tau_1/[1 + (\omega\tau_1)2] + {S_f}^2(1 - {S_{axis}}^2)\tau_2/[1 + (\omega\tau_2)^2].$$

In the equations above, τ_m is the overall rotational time and an isotropic overall motion is assumed; $1/\tau_1 = 1/\tau_m + 1/\tau_f$, $1/\tau_2 = 1/\tau_m + 1/\tau_{axis}$, τ_f is the correlation time for methyl rotation about the symmetric axis, τ_{axis} is the correlation time for reorientation of the methyl symmetric axis; $S^2 = {S_{axis}}^2{S_f}^2$; ${S_f}^2 = P_2(\cos(\theta_{ij}))\ P_2(\cos(\theta_{kl}))$, θ_{ij} (θ_{kl}) the angle between bond ij (kl) and the symmetrical axis (Kay and Torchia, 1991); ${S_{axis}}^2$ is the order parameter of the symmetrical axis of methyl group; $\mathbf{u}_{ij}$ is a unit vector describing the orientation of interaction vector **ij** in a frame that is fixed in the macromolecule; $\mathbf{u}_i$ is a unit vector describing the orientation of axially symmetric CSA tensor in the molecular frame; γ is the gyromagnetic ratio; h is Planck's constant; μ_0 is permeability of a vacuum; r_{ij} is the length between atoms i and j; $\sigma_\parallel$ and $\sigma_\perp$ are the parallel and perpendicular components of assumed axially symmetric chemical shift tensor. In the case where ij = kl, $j_{ij,kl}(\omega)$ is autocorrelation spectral density function and is denoted as $j_{ij}(\omega)$. R_{1Hsel} and R_{2H} are the longitudinal and transverse relaxation rates of methyl protons. They arise from dipolar interactions among methyl protons and their surrounding protons.

References

Bruschweiler, R., Liao, X. and Wright, P.E. (1995) *Science*, **268**, 886-889.

Bull, T. (1992) *Prog. NMR Spectrosc.*, **24**, 377–410.

Bull, T.E. (1991) *J. Magn. Reson.*, **93**, 596.

Constantine, K.L., Friedrichs, M.S., Wittekind, M., Jamil, H., Chu, C.H., Parker, R.A., Goldfarb, V., Mueller, L. and Farmer, B.T. (1998) *Biochemistry*, **37**, 7965–7980.

Daragan, V.A. and Mayo, K.H. (1993) *Biochemistry*, **32**, 11488–11499.

Delaglio, F., Grzesiek, S., Vuister, G.W., Zhu, G., Pfeifer, J. and Bax, A. (1995) *J. Biomol. NMR*, **6**, 277–293.

Dyson, H.J. and Wright, P.E. (1996) *Annu. Rev. Phys. Chem.*, **1996**(47), 369–395.

Emsley, L. and Bodenhausen, G. (1992) *J. Magn. Reson.*, **97**, 135.

Engelke, J. and Rüterjans, H. (1995) *J. Biomol. NMR*, **5**, 173–182.

Engelke, J. and Rüterjans, H. (1998) *J. Biomol. NMR*, **11**, 165–183.

Ernst, M. and Ernst, R.R. (1994) *J. Magn. Reson. Ser. A*, **110**, 202–213.

Fischer, M.W.F., Zeng, L., Pang, Y., Hu, W., Majumdar, A. and Zuiderweg, E.R.P. (1997) *J. Am. Chem. Soc.*, **119**, 12629–12642.

Garrett, D.S., Powers, R., Gronenborn, A.M. and Clore, G.M. (1991) *J. Magn. Reson.*, **95**, 214–220.

Geen, H. and Freeman, R. (1991) *J. Magn. Reson.*, **93**, 93–141.

Ghose, R. and Prestegard, J.H. (1998) *J. Magn. Reson.*, **134**, 308–314.

Goldman, M. (1984) *J. Magn. Reson.*, **60**, 437–452.

Hodsdon, M.E. and Cistola, D.P. (1997) *Biochemistry*, **36**, 1450–1460.

Ishima, R., Petkova, A.P., Louis, J.M. and Torchia, D.A. (2001) *J. Am. Chem. Soc.*, **123**, 6164–6171.

Kay, L.E. and Bull, T.E. (1992) *J. Magn. Reson.*, **99**, 615–622.

Kay, L.E. and Petsko, A.G. (2001) *Curr. Opin. Struct. Biol.*, **11**, 513–515.

Kay, L.E. and Torchia, D.A. (1991) *J. Magn. Reson.*, **95**, 536.

Kay, L.E., Bull, T.E., Nicholson, L.K., Griesinger, C., Schwalbe, H., Bax, A. and Torchia, D.A. (1992a) *J. Magn. Reson.*, **100**, 538–558.

Kay, L.E., Keifer, P. and Saarinen, T. (1992b) *J. Am. Chem. Soc.*, **114**, 10663–10665.

Kay, L.E., Muhandiram, D.R., Farrow, N.A., Aubin, Y. and Forman-Kay, J.D. (1996) *Biochemistry*, **35**, 361–368.

Kay, L.E., Torchia, D.A. and Bax, A. (1989) *Biochemistry*, **28**, 8972–8979.

Lee, A.L., Kinnear, S.A. and Wand, A.J. (2000) *Nat. Struct. Biol.*, **7**, 72–77.

Lee, A.L., Urbauer, J.L. and Wand, A.J. (1997) *J. Biomol. NMR*, **9**, 437–440.

LeMaster, D.M. and Kushlan, D.M. (1996) *J. Am. Chem. Soc.*, **118**, 9255–9264.

Mandel, A.M., Akke, M. and Palmer, A.G. (1996) *Biochemistry*, **35**, 16009–16023.

Mayne, C.L., Grant, D.M. and Alderman, D.W. (1976) *J. Chem. Phys.*, **65**, 1684–1695.

Millet, O., Muhandiram, D.R., Skrynnikov, N.R. and Kay, L.E. (2002) *J. Am. Chem. Soc.*, **124**, 6439–6448.

Montelione, G.T., Lyons, B.A., Emerson, S.D. and Tashiro, M. (1992) *J. Am. Chem. Soc.*, **114**, 10974–10975.

Muhandiram, D.R., Yamazaki, T., Sykes, B.D. and Kay, L.E. (1995) *J. Am. Chem. Soc.*, **117**, 11536—11544.

Mulder, F.A.A., Hon, B., Muhandiram, D.R., Dahlquist, F.W. and Kay, L.E. (2000) *Biochemistry*, **39**, 12614–12622.

Nesmelova, I., Krushelnitsky, A., Idiyatullin, D., Blanco, F., Ramirez-Alvarado, M., Daragan, V.A., Serrano, L. and Mayo, K.H. (2001) *Biochemistry*, **40**, 2844—2853.

Nicholson, L.K., Kay, L.E., Baldisseri, D.M., Arango, J., Young, P.E., Bax, A. and Torchia, D.A. (1992) *Biochemistry*, **31**, 5253–5263.

Onuchic, J.N., Luthey-Schulten, Z. and Wolynes, P.G. (1997) *Annu. Rev. Phys. Chem.*, **48**, 545–600.

Palmer, A.G. (2001) *Annu. Rev. Biophys. Biomol. Struct.*, **30**, 129–155.

Palmer, A.G., Rance, M. and Wright, P.E. (1991) *J. Am. Chem. Soc.*, **113**, 4371–4380.

Palmer, A.G., Williams, J. and McDermott, A. (1996) *J. Phys. Chem.*, **100**, 13293–13310.

Redfield, A.G. (1957) *IBM J. Res. Dev.*, **1**, 19.

Reif, B., Hennig, M. and Griesinger, C. (1997) *Science*, **276**, 1230–1233.

Stites, W.E. (1997) *Chem. Rev.*, **97**, 1233–1250.

Tjandra, N., Szabo, A. and Bax, A. (1996) *J. Am. Chem. Soc.*, **118**, 6986–6991.

Wand, A.J. (2001) *Nat. Struct. Biol.*, **8**, 926–931.

Wand, A.J., Urbauer, J.L., McEvoy, R.P. and Bieber, R.J. (1996) *Biochemistry*, **35**, 6116–6125.

Yamazaki, T., Muhandiram, D.R. and Kay, L.E. (1994) *J. Am. Chem. Soc.*, **116**, 8266–8278.

Yang, D.W., Konrat, R. and Kay, L.E. (1997) *J. Am. Chem. Soc.*, **119**, 11938–11940.

Yang, D.W., Mittermaier, A., Mok, Y.K. and Kay, L.E. (1998) *J. Mol. Biol.*, **276**, 939–954.

Yang, D.W., Mok, Y.K., Muhandiram, D.R., Forman-Kay, J.D. and Kay, L.E. (1999) *J. Am. Chem. Soc.*, **121**, 3555–3556.

Ye, C., Fu, R., Hu, J., Hou, L. and Ding, S. (1993) *Magn. Reson. Chem.*, **31**, 699–704.

Zhang, F., Lucke, C., Baier, L.J., Sacchettini, J.C. and Hamilton, J.A. (1997) *J. Biomol. NMR*, **9**(213–228).

Zheng, Z.W., Mayne, C.L. and Grant, D.M. (1993) *J. Magn. Reson. Ser. A*, **103**, 268.